

Comparative performance of Salinity gradient power-reverse electrodialysis under different operating conditions

Accepted Manuscript

Desalination

5 January 2019

Rafael Ortiz-Imedio, Lucia Gomez-Coma, Marcos Fallanza, Alfredo Ortiz,
Raquel Ibañez, Inmaculada Ortiz*
Department of Chemical and Biomolecular Engineering, University of Cantabria, Av. Los Castros 46,
39005 Santander, Spain
*corresponding author: ortizi@unican.es

Abstract

Promotion of renewable energies to substitute carbon-based energy has boosted the development of new membrane technologies based on Salinity Gradient Power (SGP) by Reverse Electrodialysis (RED). This paper is focused on providing a useful, feasible and robust tool for the design of this technology, able to predict the behaviour under different operational conditions, critical for RED performance. Therefore, open circuit voltage (OCV), internal resistance (R_i) and gross power (P) are evaluated. Furthermore, the model predictability has been validated with experimental results obtained working with three cases of study corresponding to seawater/WWTP effluent, brines/brackish water and an intermediate concentration gradient scenario. Feed flow rate (Reynolds numbers from 2.7 to 13.6), and temperature (from 286 K to 297 K) have been also tested in a lab-scale set-up with 0.4 m² of membrane area; the maximum power achieved at 297±1 K was 0.66 W, 1.6 W and 0.3 W for the three cases respectively. The results highlight the strong influence of temperature and the dominance of the low compartment resistance on the process performance; thus, working with the highest possible SG does not always provide the best outcome, but a trade-off between SG and resistance of the dilute solution should be searched.

Keywords (max 5): Reverse Electrodialysis (RED), Salinity Gradient (SG), Ion Exchange Membrane (IEM), Gross Power, Internal Resistance

1. Introduction

The rising energy demand and the great dependence on fossil fuels leads to the investigation of clean and renewable energies. The main strategy is to avoid thermal and environmental pollution, as well as emission of greenhouse gases and generation of radioactive wastes [1–4]. Salinity Gradient Power (SGP), also named “Blue Energy”, is one of these energy sources. SGP is based on the physico-chemical potential existing when two water streams of different salinity are mixed. Globally, there is an amount of energy theoretically available between 1.4 - 2.6 TW based on the rivers discharges into oceans [5]. The main technology to harvest the SGP energy is the Reverse Electrodialysis (RED), which converts the blue energy into electricity through ion exchange membranes (IEMs) [6–8].

The number of publications about RED has increased exponentially in the last decade [9]. The RED technology is based on the conventional electrodialysis (ED) technology. However, the ED is a separation technique that uses an electric current as input to desalinate water or to recover dissolved salts moving the ions through the IEMs against the chemical potential [10]. On the other hand, RED generates electrical energy mixing two streams of different salinity in a controlled way allowing the ions to move from the concentrated solution to the diluted one through membranes [11].

A conventional cell pair in a RED stack is the essential unit that repeats inside and consists of a cation exchange membrane (CEM), a spacer, an anion exchange membrane (AEM) and another spacer for the concentrated solution compartment. The CEMs allow the transport of cations, mainly Na^+ , while the AEMs are permeable to anions, primarily Cl^- . Spacers are mesh of filaments usually placed between the membranes to keep the distance, to create compartments for the flow of the water streams and to promote turbulence [12–14]. However, both the pressure drop and the resistance to ions transport are increased [9,11]. The alternating flows of concentrated and diluted solutions throughout the stack, results in an electric potential difference over each membrane [15,16]. At the ends of the stack, the electrodes (anode and cathode) convert the ion flux into electric current by means of a suitable redox couple [17]. Generally, there is no net chemical reaction: the oxidation at the anode is balanced with the reduction at the cathode, flowing constantly the electrode rinse solution in a closed loop. In a laboratory scale an external load connected to the electrodes by an outer circuit consumes the electrical power

generated inside the stack [18]. Working in pilot or industrial scale it is possible connecting the power to the electricity grid.

Despite the global theoretical power of the SGP, this technology is still largely underdeveloped. Only two pilot plants which use the RED technology are currently working: one in Afsluitdijk, The Netherlands, by the company REDstack B.V., and the second one in Marsala, Italy, within the European project REAPower [7]. The former, inside the project Blue Energy, was installed in 2014 with a target of 50 kW gross power generation. The flow rates are around $220 \text{ m}^3 \cdot \text{h}^{-1}$ of seawater ($0.479 \text{ mol} \cdot \text{L}^{-1}$) and freshwater ($0.0034 - 0.0086 \text{ mol} \cdot \text{L}^{-1}$), respectively [19]. The latter plant has 3 RED units with approximately 400 m^2 of total membrane area. REAPower uses brines ($3.422 - 5.133 \text{ mol} \cdot \text{L}^{-1}$) from saltworks and brackish water ($0.034 - 0.051 \text{ mol} \cdot \text{L}^{-1}$) from a shoreline well. Nowadays, the pilot plant has a nominal power capacity of 1 kW, reaching a gross power of 330 W with real solutions [13]. This pilot plant demonstrates the possibility of harvesting energy from other sources of water such as brines, brackish water or treated municipal wastewater, instead of the conventional saline gradient seawater/river water. Further research is needed to develop RED stacks optimised for the diverse possible scenarios [20]. Recently, several works have focused on the application of the technology at laboratory scale to different streams such as brines/river water [21,22], brines/brackish water [7,8,11,13,19], brines/seawater [12,23,24], seawater/river water [4,11,14,25–27] or seawater/wastewater [20,28].

Nowadays, the efforts to develop more efficient RED processes are focused on two ways. On the one hand, improving the stack components providing new membrane types, as well as optimal fluid dynamic spacers [29–33]. On the other hand, providing an effective tool able to predict the influence of the operation variables on the technology performance and process costs.

The main operation variables have been studied in the literature in order to determine the optimal technology output as function of feed water characteristics. In terms of concentration, for a given high concentration solution (HC), higher values of LC (low concentration solution) result in two competing effects: reduced electromotive force that would reduce power output performance but lower internal resistance that would promote more power generation. In addition, concentration polarization and both, non-ohmic and solution resistances, are reduced [7,12,22–26,29]. Regarding feed flow rates, Reynolds

numbers from 0 to 20 have been studied by different authors. Increment velocities implies higher electric potential values and lower polarization effects but an increase in the LC solution resistance. The effect of increasing gross power is mainly due to the lower residence time, leading to a larger concentration difference along the stack [11,14,31–39]. However, higher flow rates lead to an increase in pressure drop and pumping power. Finally, the influence of temperature has been also considered [6,9,22,24,30,40,41]. Previous works have carried out experiments in the range from 283 K to 333K, reaching greater gross power values but lower permselectivity when temperature increases. Furthermore, rising temperature implies a positive effect on the conductivity of saline solutions, diffusivity and membrane resistances.

The availability of a comprehensive model that allows predicting and optimizing the performance of the system under different operation conditions would constitute a very useful and powerful tool for the decision-making process. Up to now interesting works have reported the simulation of the flow rate ratios effect [35,47,48], streams' concentration [35,47,48], multivalent ion compositions [39] and temperature [49] on the power and stack open circuit voltage (OCV). On the other hand, several authors work on stack design and optimization through CFD models that simulate the flow pattern and study the influence of flow rates, solution concentration, mass transfer rate, profiled membranes or spacer configurations [8,41,42,50,51]. Finally, some works consider the stack elements characteristics, such as the membrane resistances [52,53] or the pressure drop [25].

Gathering the information previously reported, this work aims to go one step further in developing a broad vision mathematical model able to predict the performance of RED technology to the recovery of SGP under different scenarios. In this sense, the model based on the Nernst, flux and mass balance equations, properly addresses the comparison of RED performance under different operating conditions and provides an efficient tool for decision-making in the implementation of the technology. The model evaluates open circuit voltage (OCV), internal resistance (R_i) and gross power (P) and highlights the relevance of searching a trade-off between salinity gradient and resistance of the low concentration compartment on the optimum RED performance.

For this purpose, the mathematical model together with the characteristic parameters, that account for the module geometry, diffusivities and membrane resistances and

permselectivities, has been implemented and solved with the software Aspen Custom Modeler®. The model has been validated by experimental data obtained in a laboratory scale plant working with model solutions representative of different SG scenarios: case C1, corresponding to seawater/wastewater (0.66 M/0.0036 M); C2, brines/brackish water (5 M/0.1 M); and C3, an intermediate scenario (5 M/1 M). Moreover, using case C1, an analysis by means of different temperatures and flowrates has been performed.

2. Experimental and Modelling

2.1 RED Stack

A RED stack was tested for a set of experiments outfitted with 20 pairs of Ion Exchange Membranes (IEMs) supplied by Fumatech (Fumatech®, Germany). The membrane area per cell was 200 cm². Relevant characteristics of Fumasep membranes FAS-50 as AEM and FKS-50 as CEM, are reported in Table 2. Both membranes have low values of resistance and high permselectivity, features that favour their application in RED experiments [9,11]. High permselectivity values of membranes allow the suitable ion flux from concentrate to dilute channels [13].

Table 2. Main membrane characteristics

Membrane	Thickness (μm)	Permselectivity 0.1-0.5M (%)	Area resistance (Ω·cm ²)
FAS-50 (AEM)	45-55	92-96	0.6-1.5
FKS-50 (CEM)	45-55	97-99	1.8-2.5

Commercial polyethersulfone (PES) spacers of 270 μm were used to separate the membranes with a porosity value of 82.5%. Finally, the electrodes were composed of titanium/mixed oxides. Table 3, summarizes the main RED stack specifications. Fig. 1a, shows a schematic of the system used in this work while Fig. 1b shows a cell pair of the stack.

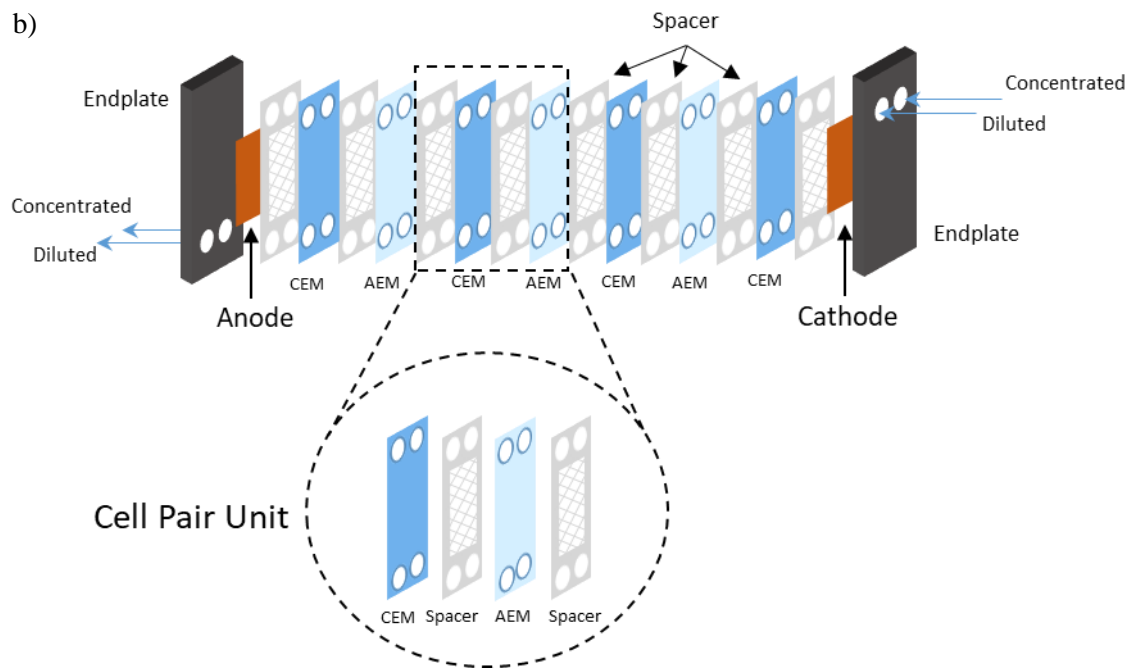
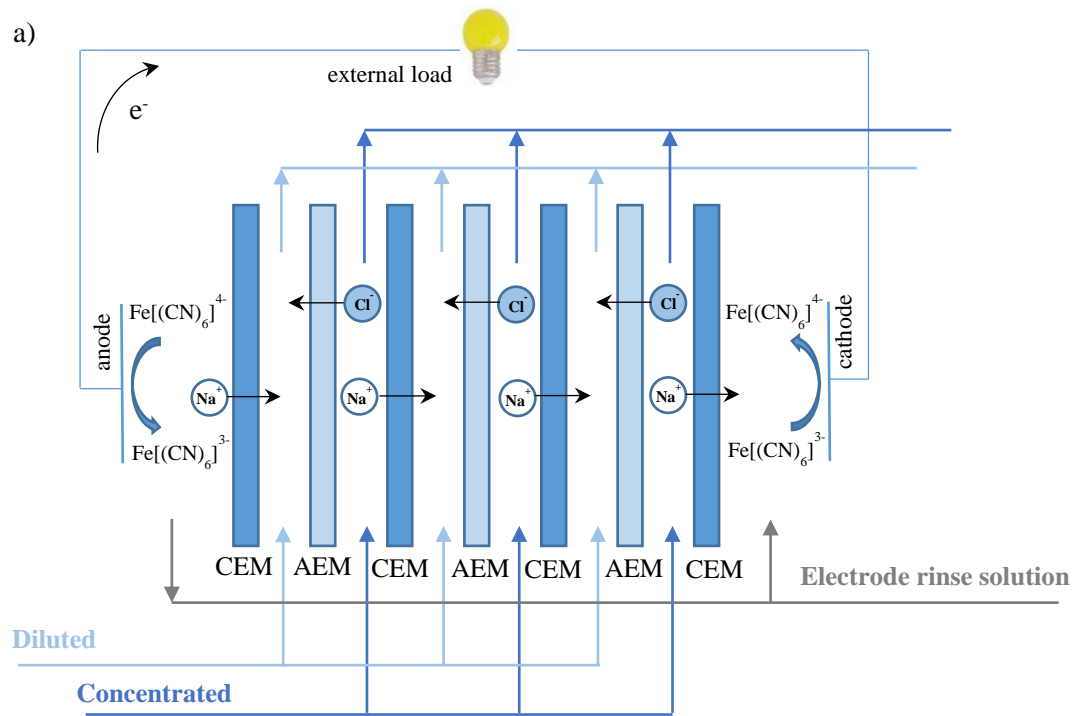


Fig. 1. RED stack a) schematic of the system b) cell pair

Table 3: RED stack specifications

	Value
Area of one membrane (m ²)	0.02
Cell width (m)	0.063
Cell length	0.32
Intermembrane distance (m)	$5 \cdot 10^{-5}$
Membrane pairs (-)	20

2.2 Methods

Feed solutions were prepared using industrial grade Sodium chloride (assay >99.5) provided by Fisher Chemicals, Spain and distilled water. The stack was continuously fed with stream solutions. Three different cases of concentration gradient were used. The low concentrated solution (LC) was varied from NaCl 0.0036 M, typical average value in municipal wastewater coming from WWT plants, to NaCl 1 M. The high concentrated solution (HC) was ranged from NaCl 0.66 M corresponding to seawater to NaCl 5 M (concentrated brines). Table 4 summarizes the experimental conditions. Flow rates (Q) were varied from 2.7 to 13.6 Reynolds number. Furthermore, different temperatures were tested, 286 ± 1 K corresponding to the seawater temperature in winter, 291 ± 1 K, and 297 ± 1 K analogous to the temperature in summer.

Table 4. Experiments accomplished.

Q _{HC}	Q _{LC}	C _{HC} / C _{LC}	T
100-500 mL·min ⁻¹ (Re=2.7-13.6)		C1: 0.66 M / 0.0036 M	297 ± 1 K
200 mL·min ⁻¹ (Re=5.4)	100-150 mL·min ⁻¹ (Re=2.7-4.1)	C1: 0.66 M / 0.0036 M	297 ± 1 K
100-150 mL·min ⁻¹ (Re=2.7-4.1)	200 mL·min ⁻¹ (Re=5.4)	C1: 0.66 M / 0.0036 M	297 ± 1 K
200 mL·min ⁻¹ (Re=5.4)		C2: 5 M / 0.1 M	297 ± 1 K
200 mL·min ⁻¹ (Re=5.4)		C3: 5 M / 1 M	297 ± 1 K
200 mL·min ⁻¹ (Re=5.4)		C1: 0.66 M / 0.0036 M	286 ± 1 K
200 mL·min ⁻¹ (Re=5.4)		C1: 0.66 M / 0.0036 M	291 ± 1 K

Fig. 2 shows the experimental setup of the laboratory plant. Both HC and LC solutions were pumped into the RED stack using two peristaltic pumps (Watson Marlow 323E, Spain) from two tanks of 25 L each. In addition, to homogenise the solutions a rod stirrer was used. To pump the electrode rinse solution a double head peristaltic pump (Dinko Instruments D-25VXi, Spain) was employed. Moreover, in order to control the HC and LC concentration two conductivimeters were utilised (Hach Sension+ EC71, Spain) and to check the pH in the ERS (electrode rinse solution) a pHmeter was used (Hach Sension+ PH31, Spain). The ERS was composed of 0.05 M $K_3Fe(CN)_6$, 0.05 M $K_4Fe(CN)_6$ (Scharlau, purity >99.0%), and 0.25 M NaCl (Fisher Chemicals, assay >99.5%). ERS was continuously recirculated through the electrode compartments at a flow rate of 300 mL·min⁻¹.

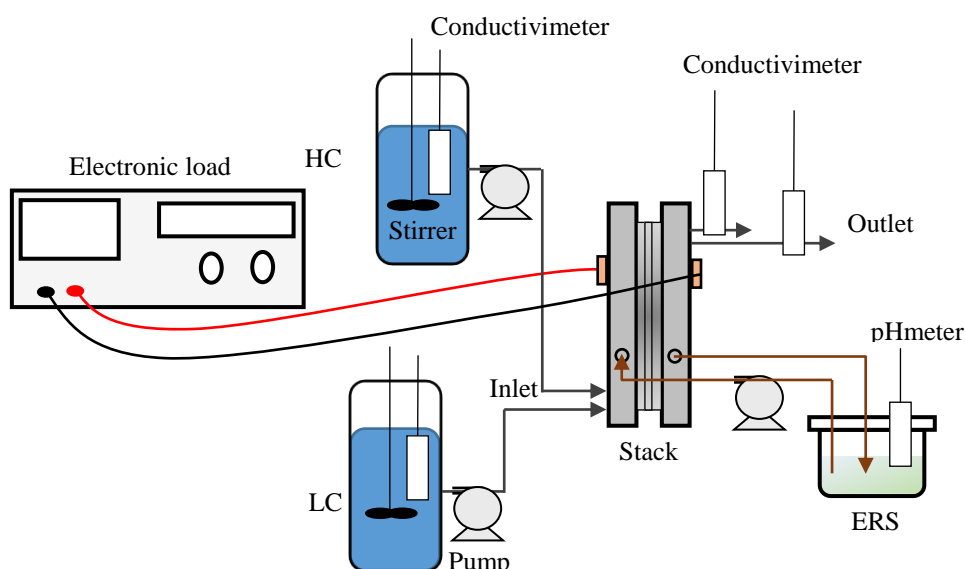


Fig. 2. Lab-scale experimental setup

Experiments were performed using an electronic load in the galvanostatic mode (Chroma Systems Solutions 63103A, USA). The RED stack was kept in open circuit mode for almost 5 min to reach steady state. Then, the electrical current was modified in steps of 0.025 A, from 0 to 1 A measuring the voltage produced. Each current value was maintained until the voltage was constant. Every experiment was repeated at least two times as independent tests.

2.3 Model development

To carry out the modelling, the simulation tool Aspen Custom Model V9 (AspenTech) was used based on the equations that describe the phenomena occurring inside the cell [22,35,47,54,55]. In this work a robust model is proposed as a useful tool that allows the study of the main operation variables such as flow rates, concentration and temperature. The model has been discretised along the cell length (L) using steps of 0.005 m. The following considerations have been established: (i) co-current flow distribution, (ii) both streams are purely sodium chloride aqueous solutions and, (iii) the parameters required to obtain a final value (such as gross power) are evaluated at the average conditions between inlet and outlet of the feed channels. Additionally, the following assumptions were adopted: the electrode rinse solution is in excess and the membrane properties are kept constant along the experiment. Thus, the cell pair voltage can be evaluated through the Nernst equation [35,39]:

$$E_{cell}(x) = \alpha_{CEM} \cdot \frac{R \cdot T}{F} \cdot \left[\frac{1}{z_i} \ln \left(\frac{\gamma_{HC}^{Na^+}(x) \cdot C_{HC}^{Na^+}(x)}{\gamma_{LC}^{Na^+}(x) \cdot C_{LC}^{Na^+}(x)} \right) \right] + \alpha_{AEM} \cdot \frac{R \cdot T}{F} \cdot \left[\frac{1}{z_{ion}} \ln \left(\frac{\gamma_{HC}^{Cl^-}(x) \cdot C_{HC}^{Cl^-}(x)}{\gamma_{LC}^{Cl^-}(x) \cdot C_{LC}^{Cl^-}(x)} \right) \right] \quad (1)$$

Where α_{CEM} and α_{AEM} are the permselectivity of cation and anion membranes respectively, F is the Faraday's constant (96,485 C mol⁻¹), R is the Universal gas constant (8.314 J·mol⁻¹·K⁻¹), T is the temperature (K), C is the ion concentration (mol·m⁻³) and z is the valence. Moreover, γ is the activity coefficient. This coefficient is determined by Debye Hückel (0 < C < 1 M) [47] or Pitzer (C > 1 M) equations [35,56].

Fig. 3 shows the equivalent electrical circuit. When the stack is connected to an external load (R_L), the voltage output (E) can be calculated as the theoretical voltage from all the stack cell pairs minus the voltage drop across the total internal resistance in the stack (R_{stack}) [9].

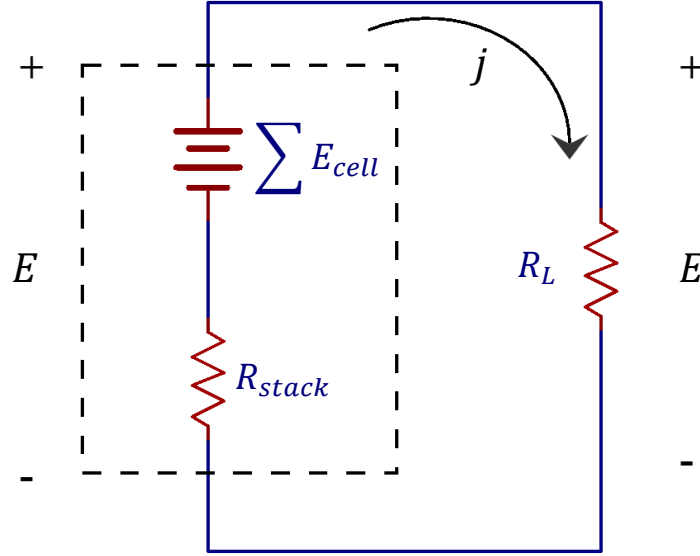


Fig. 3. Equivalent electrical circuit.

$$E = \sum E_{cell} - j \cdot R_{stack} \quad (2)$$

In Eq. (2) E is in V, $\sum E_{cell}$ is the sum of all the cell pair voltages (V), j is the electrical current density ($A \cdot m^{-2}$) and R_{stack} is the sum of all the cell pairs internal resistances ($\Omega \cdot m^2$). On the other hand, the voltage output is equal to the voltage drop in the external load:

$$E = j \cdot R_L \quad (3)$$

With R_L as the external load ($\Omega \cdot m^2$).

From Fig. 3 and equations 2 and 3, the current density discretised along the compartment length can be determined with the following equation:

$$j(x) = \frac{\sum E_{cell}(x)}{R_{stack}(x) + R_L} \quad (4)$$

The gross power, P , in (W) is calculated as the product of the output voltage and the electrical current, as shown in equation 5. The current has been calculated as the product of the average current density along the cell length and the membrane area.

$$P = E \cdot I \quad (5)$$

The resistance of a RED stack is the addition of the different resistances of each cell pair in series [55]. Inside them, the internal loss, R_i in ($\Omega \cdot m^2$), could be mainly divided into an ohmic part and a non-ohmic part as can be seen in equation 6 [4,9]. Furthermore, R_i could be determined experimentally using the electronic load. Vermaas et al. explained this procedure in detail in previous works [11,54,57].

$$R_i(x) = R_{ohmic}(x) + R_{non-ohmic}(x) \quad (6)$$

Equation 7 shows the ohmic resistance. R_{ohmic} is determined by the membrane resistances and compartment resistances of the high and low concentration solutions, R_{HC} ($\Omega \cdot m^2$) and R_{LC} respectively ($\Omega \cdot m^2$) [4,39,54].

$$R_{ohmic}(x) = R_{AEM} + R_{CEM} + R_{HC} + R_{LC} \quad (7a)$$

$$R_{ohmic}(x) = R_{AEM} + R_{CEM} + \frac{\delta}{\varepsilon^2 \cdot cond_{HC}(x)} + \frac{\delta}{\varepsilon^2 \cdot cond_{LC}(x)} \quad (7b)$$

Where R_{AEM} and R_{CEM} are the membrane resistances ($\Omega \cdot m^2$), ε is the porosity of the spacers (-), δ is the intermembrane distance (m) and $cond_{HC}$ and $cond_{LC}$ are the conductivities in high and low concentration compartments respectively ($S \cdot m^{-1}$).

For its part, $R_{non-ohmic}$ resistance is composed of $R_{\Delta C}$ and boundary layer resistance (R_{BL}) both in ($\Omega \cdot m^2$) as it is shown in the next equation:

$$R_{non-ohmic}(x) = R_{\Delta C}(x) + R_{BL}(x) \quad (8)$$

$R_{\Delta C}$ is the contribution to the resistance due to the concentration change in the bulk solution along the compartments between the inlet and the outlet. This resistance is calculated based on equation 9 [11,21,55].

$$R_{\Delta C}(x) = \frac{\alpha \cdot R \cdot T}{z \cdot F \cdot j(x)} \cdot \ln\left(\frac{\Delta_{LC}}{\Delta_{HC}}\right) = \frac{\alpha \cdot R \cdot T}{z \cdot F \cdot j(x)} \cdot \ln\left(\frac{1 + \frac{j(x) \cdot A}{F \cdot Q_{LC}(x) \cdot C_{LC}(x)}}{1 - \frac{j(x) \cdot A}{F \cdot Q_{HC}(x) \cdot C_{HC}(x)}}\right) \quad (9)$$

Where A is the area of one membrane (m^2), α is the average permselectivity (-), and Q is the volumetric flow rate per cell ($m^3 \cdot s^{-1}$), .

Finally, R_{BL} is the boundary layer resistance due to the concentration polarization ($\Omega \cdot m^2$) [44]. This contribution can be calculated for each compartment using the equation reported by Vermass [54].

$$R_{BL}(x) = 10^{-3} \cdot \left(0.62 \cdot \frac{tr(x) \cdot \delta}{L} + 0.05 \right) \quad (10)$$

In which tr is the residence time (s) calculated as described by the equation 11, δ is the intermembrane thickness and L is the cell length (m).

$$tr(x) = \frac{L \cdot b \cdot \delta \cdot \varepsilon}{Q(x)} \quad (11)$$

Where b is the cell width.

The total flux is generated by Na^+ cations crossing the cation exchange membranes and Cl^- anions going through the anion exchange membranes, both from the concentrated to the diluted solutions. This can be expressed according to equations 12a and 12b:

$$J_{Na^+}(x) = \frac{j(x)}{F} + \frac{D_{NaCl}}{\delta_m} (C_{HC}^{Na^+}(x) - C_{LC}^{Na^+}(x)) \quad (12a)$$

$$J_{Cl^-}(x) = \frac{j(x)}{F} + \frac{D_{NaCl}}{\delta_m} (C_{HC}^{Cl^-}(x) - C_{LC}^{Cl^-}(x)) \quad (12b)$$

Where D_{NaCl} is the salt diffusivity ($m^2 \cdot s^{-1}$), and δ_m is the membrane thickness (m).

The water transport through ion exchange membranes is due to the osmotic flux [35,39]. The water flux moves from low to high concentrated solution and is described by the following equation:

$$J_{H_2O}(x) = \frac{2D_{H_2O}}{\delta_m} \left((C_{HC}^{Na^+}(x) + C_{HC}^{Cl^-}(x)) - (C_{LC}^{Na^+}(x) + C_{LC}^{Cl^-}(x)) \right) \quad (13)$$

In which J_{H_2O} is the osmotic flux ($mol \cdot m^{-2} \cdot s^{-1}$), D_{H_2O} is the water diffusivity ($m^2 \cdot s^{-1}$).

The water and ions fluxes cause variation in the salt concentration of the solutions along the compartments, described through their mass balance equations:

$$\frac{dC_{HC}^{Na^+}(x)}{dx} = -\frac{b}{Q_{HC}(x)} \cdot J_{Na^+}(x) - C_{HC}^{Na^+}(x) \cdot \frac{b \cdot J_{H_2O}(x)}{Q_{HC}(x)} \cdot V_{H_2O} \quad (14a)$$

$$\frac{dC_{HC}^{Cl^-}(x)}{dx} = -\frac{b}{Q_{HC}(x)} \cdot J_{Cl^-}(x) - C_{HC}^{Cl^-}(x) \cdot \frac{b \cdot J_{H_2O}(x)}{Q_{HC}(x)} \cdot V_{H_2O} \quad (14b)$$

$$\frac{dC_{LC}^{Na^+}(x)}{dx} = \frac{b}{Q_{LC}(x)} \cdot J_{Na^+}(x) + C_{LC}^{Na^+}(x) \cdot \frac{b \cdot J_{H_2O}(x)}{Q_{LC}(x)} \cdot V_{H_2O} \quad (14c)$$

$$\frac{dC_{LC}^{Cl^-}(x)}{dx} = \frac{b}{Q_{LC}(x)} \cdot J_{Cl^-}(x) + C_{LC}^{Cl^-}(x) \cdot \frac{b \cdot J_{H_2O}(x)}{Q_{LC}(x)} \cdot V_{H_2O} \quad (14d)$$

Where V_{H_2O} is the water molar volume ($m^3 \cdot mol^{-1}$) [47]. As can be seen in the equations 14a and 14b, in the HC compartment the concentration decreases because the ions move to the LC compartment and there is an inflow of water from the diluted to the concentrated compartment due to osmosis. In the LC solution (Eq. 14c and 14d) the opposite effect takes place .

The water flux, besides changing the salt concentration of the solutions, it also slightly modifies the flow rates of both compartments, increasing in the concentrated and diminishing in the diluted one [47], as shown in equations 15a and 15b:

$$\frac{dQ_{HC}(x)}{dx} = b \cdot J_{H_2O}(x) \cdot V_{H_2O} \quad (15a)$$

$$\frac{dQ_{LC}(x)}{dx} = -b \cdot J_{H_2O}(x) \cdot V_{H_2O} \quad (15b)$$

The Reynolds number (Re) can be used to indicate the fluid dynamic regime inside each compartment in a standard way. Re can be formulated through equation 16. The hydraulic diameter is twice the intermembrane distance and is corrected with the porosity for the volume filled by the spacer [43].

$$Re(x) = \frac{v \cdot D_h \cdot \rho}{\mu} = \frac{2 \cdot Q(x) \cdot \rho}{\varepsilon \cdot b \cdot \mu} \quad (16)$$

Where v is the velocity ($m \cdot s^{-1}$), D_h is the hydraulic diameter (m), ρ is the density of the solutions ($kg \cdot m^{-3}$) and μ is the dynamic viscosity ($kg \cdot m^{-1} \cdot s^{-1}$).

The equations are closely interconnected and are strongly influenced by the operation variables flow rate (Q), concentration (C), and temperature (T). Modifications on a variable affect implicitly to nearly all equations, increasing the complexity of the model.

3. Results and discussion

In this section, the effect of the feed flow rate, salinity gradient and temperature on a RED stack is studied in terms of open circuit voltage, internal resistance, current voltage and power curves. Moreover, the model presented is validated through the comparison between experimental and simulated results.

3.1. Feed flow rate

The feed flow rate influence was assessed in the range of Reynolds numbers from 2.7 to 13.6 in the cases of equal and different flow rates in the HC and LC solutions. The scenario C1: seawater (NaCl 0.66 M)/WWTP effluent (NaCl 0.0036 M) was used and the temperature was kept constant at 297 ± 1 K.

The simulations were done using the parameters reported in Tables 2 and 3 as well as the set of equations presented above. D_{NaCl} and $D_{\text{H}_2\text{O}}$ were estimated fitting the experimental results to the simulated data for the type of membranes selected at 297 K. The values reported were $D_{\text{NaCl}}=4.56 \cdot 10^{-12} \text{ m}^2 \cdot \text{s}^{-1}$ and $D_{\text{H}_2\text{O}}=1.01 \cdot 10^{-10} \text{ m}^2 \cdot \text{s}^{-1}$ which are in concordance with literature [58].

Table 5 shows the experimental and simulated open circuit voltage (OCV) values as well as the error achieved between both values, which are in good agreement. An increase in the feed flow rates leads to higher OCV because the residence time for ion exchange is lower keeping higher salinity gradient along the cell. In addition, the concentration polarization decreases. When $Q_{\text{HC}} \neq Q_{\text{LC}}$, OCV is more strongly influenced by LC as the concentration is lower and small changes have stronger repercussion (Table 5). The maximum error obtained was 2.82% corresponding to Reynolds numbers of HC $\text{Re}=2.7$ and LC $\text{Re}=5.4$.

Table 5. Experimental and simulated OCV values.

mL·min ⁻¹ (Re)	Exp. (V)	Sim. (V)	Error (%)
HC=LC=100 (2.7)	3.77	3.79	0.53
HC=LC=200 (5.4)	4.11	4.15	0.97
HC=LC=300 (8.1)	4.28	4.31	0.70
HC=LC=400 (10.9)	4.37	4.41	0.92
HC=LC=500 (13.6)	4.40	4.47	1.59
HC=100 LC=200 (2.7-5.4)	4.26	4.14	2.82
HC=150 LC=200 (5.4-4.1)	4.04	4.14	2.48
HC=200 LC=150 (4.1-5.4)	4.03	4.02	0.25
HC=200 LC=100 (5.4-2.7)	3.85	3.80	1.30

The internal resistance per cell (R_i), is plotted against the current intensity and Re in Fig. 4. Simulated values are able to describe the experimental behaviour. In addition, the different contributions (%) of each individual resistance to the internal resistance per cell as function of the Reynold number at maximum gross power are shown in Fig. 5 as well as the contribution to the total ohmic resistance (%).

When the electric current is close to zero the internal resistance increases for higher residence times because $R_{\Delta C}$ resistance is dominant (Fig. 4a). As the electrical current is risen, $R_{\Delta C}$ is less relevant as can be seen in Eq. 9, and hence, the curves cross each other (Fig. 5). In general terms, R_i increases as the flow rate is incremented and decreases with the current intensity due to the lower salt concentration in LC.

Fig. 4b shows the relationship between the internal resistance and different flow rates in each compartment. Keeping constant the flow rate in the low concentrated solution, R_i is maintained. When HC_Re=2.7-5.4 and LC_Re=5.4 were used, R_i values overlapped because the LC flow rate has a dominant influence on the internal resistance, particularly, in the ohmic part (Fig. 5). Different flow rates in LC imply a direct relationship between R_i and the Re number; thus, surprisingly higher Re numbers cause higher internal resistance values due to the lower concentration in this compartment.

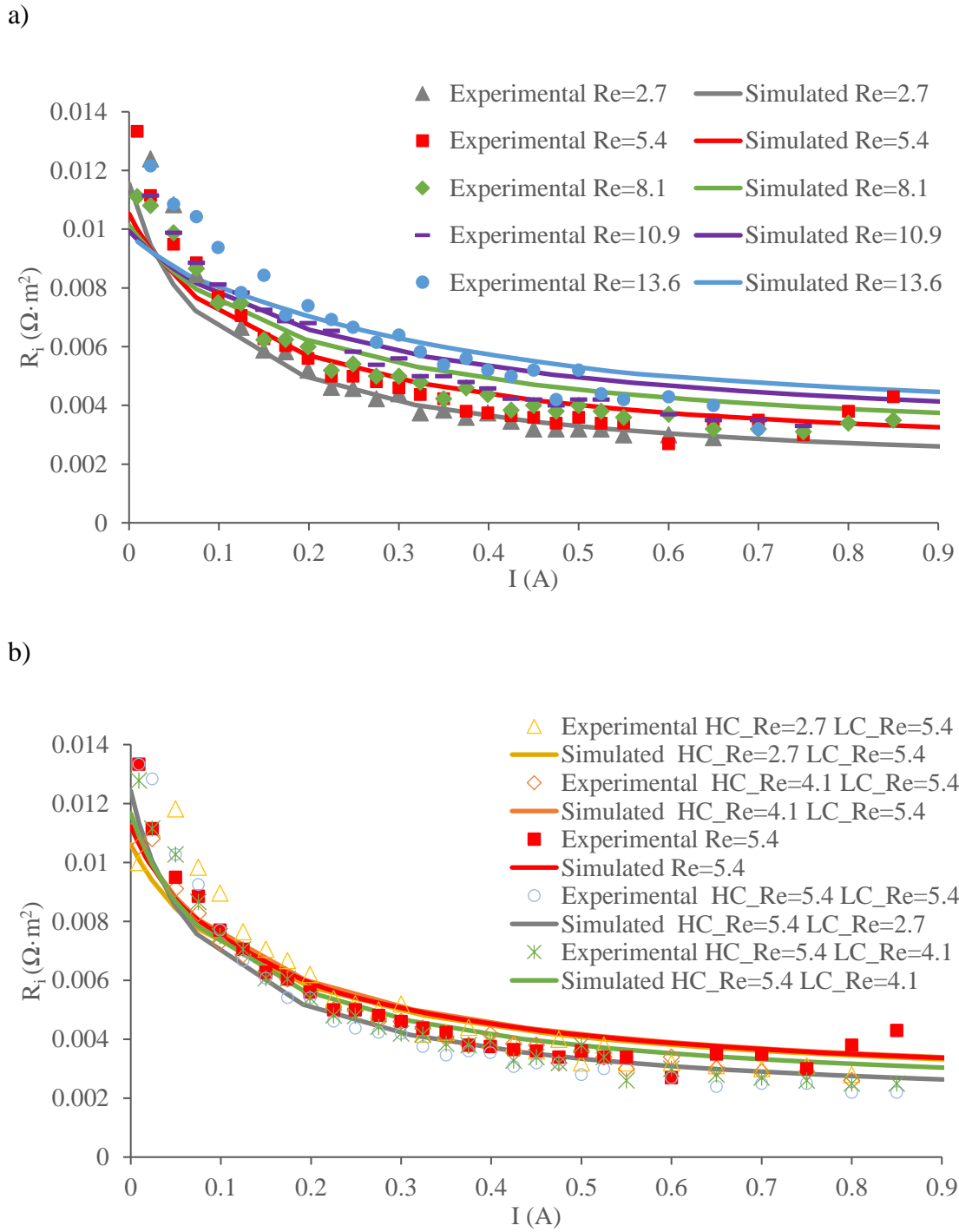


Fig. 4. Internal resistance (R_i) a) $Q_{HC}=Q_{LC}$ b) $Q_{HC}\neq Q_{LC}$

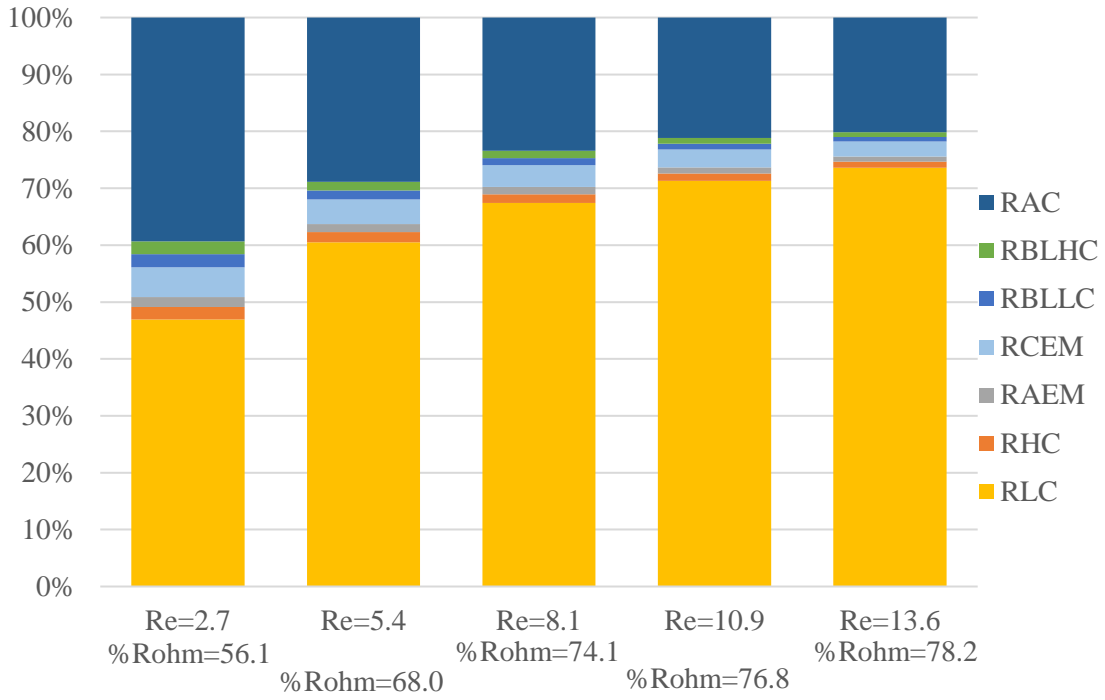
Fig. 5a illustrates the different situations when both flow rates have the same value ($Q_{HC}=Q_{LC}$). An increase in the velocity implies less ions transport through the membrane; consequently, higher resistance values in R_{LC} and higher ohmic resistance is reached. On the other hand, decreasing the residence time leads to a reduced salinity gradient along each compartment; hence lower values of $R_{\Delta C}$ are achieved. Finally, the boundary layer

resistance R_{BL} , decreases with the velocity increment because mixing is more effective at higher velocities [11]. At low flow rates, both non-ohmic and ohmic resistances are similar while $Re \geq 5.4$, R_{ohmic} is dominant.

Additionally, Fig. 5b shows the resistances' contribution when the Reynolds numbers are different in each compartment ($Q_{HC} \neq Q_{LC}$). As can be seen, a change in the flow rate has a stronger impact on the resistance of the diluted solution than on the resistance of the concentrated one. On the one hand, when $HC_Re=LC_Re=5.4$ were used, the low concentration compartment resistance had a contribution of 60%. On the other hand, when $HC_Re=5.4$ and $LC_Re=2.7$ were used the contribution of the RLC resistance decreased to 48%. Furthermore, keeping constant Q_{LC} , an increment in Q_{HC} leads to a negligible change to the different resistance contributions. This is due to the high concentration in HC and therefore, similar conductivity is maintained in the range of operation flow rates.

Fig. 6 represents the experimental (points) and simulated (lines) of total voltage (E) when $Q_{HC}=Q_{LC}$ and $Q_{HC} \neq Q_{LC}$ respectively against current showing a good prediction of experimental results. An increase in the Re number leads to higher OCV values but the limiting current decreases because of the increase in the R_i resistance, and therefore, the curve slope is incremented. Thus, the opposed effect is produced and the polarization curves cross each other as well as with the internal resistance in Fig. 4. Solely, when the flow rate corresponds to $Re=13.6$, the model prediction values slightly deviate from the experimental data. This is largely because for $Re=13.6$ the RED stack works at maximum flow rate. Keeping constant the HC flow rate, the voltage achieved is lower when the LC_Re number decreases at each current value because the higher residence time implies lower salinity gradient.

a)



b)

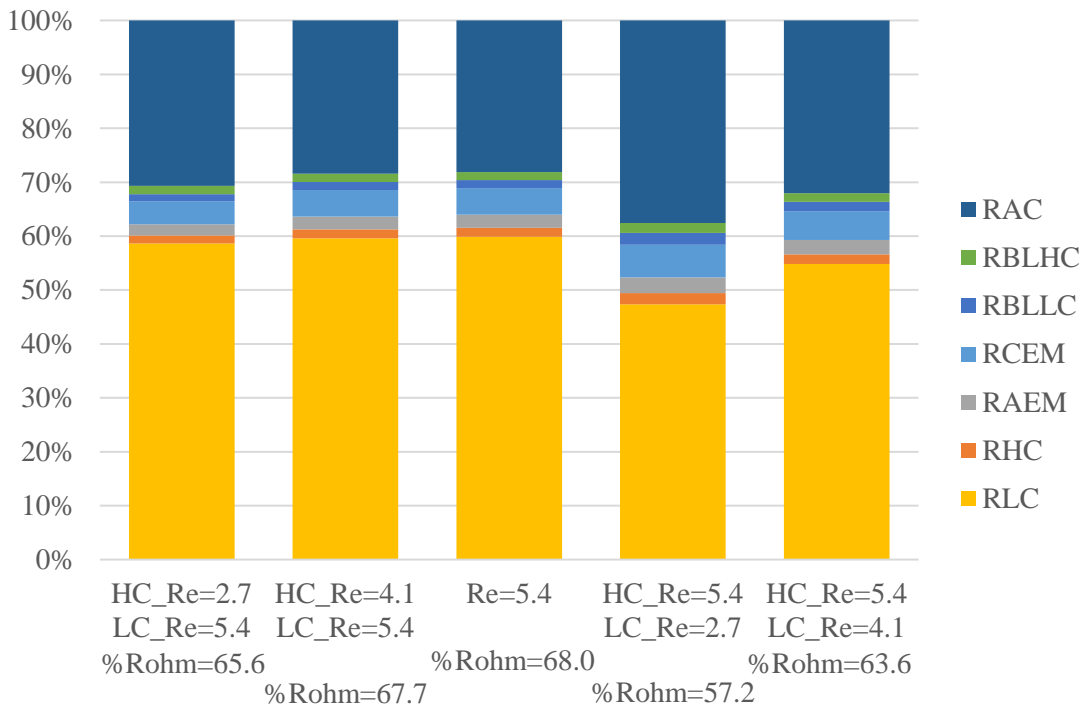
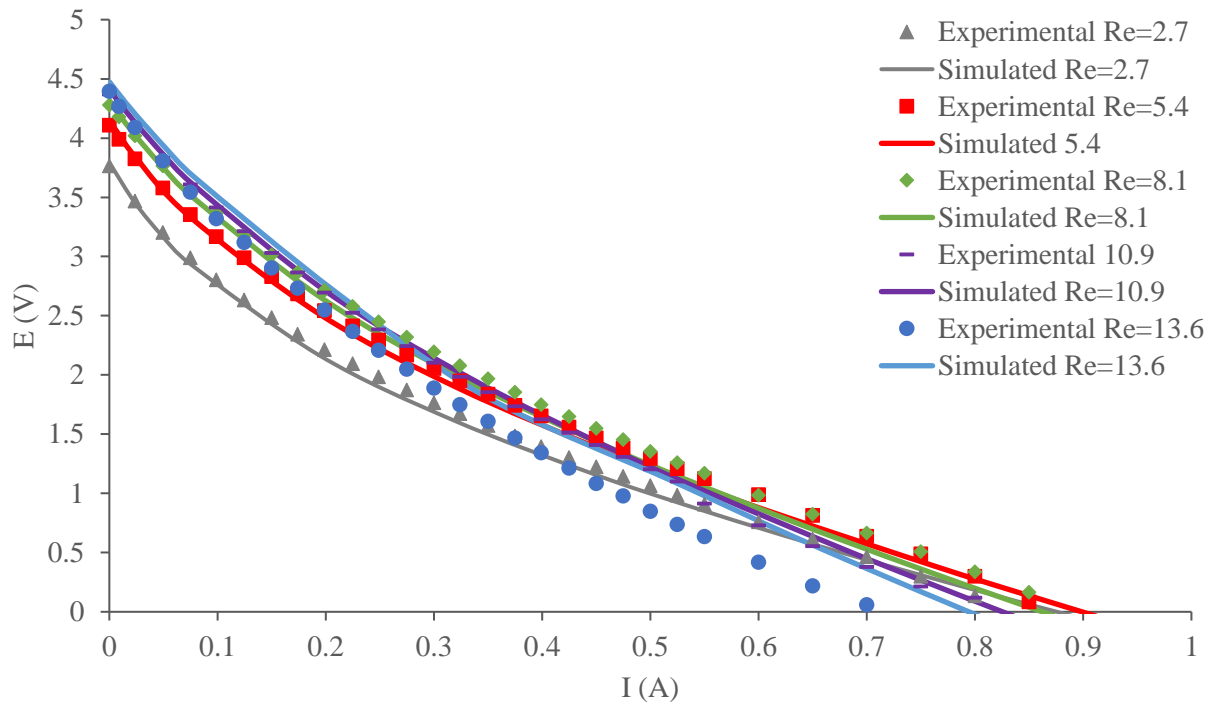


Fig. 5. Internal resistance subdivided a) $Q_{HC}=Q_{LC}$ b) $Q_{HC}\neq Q_{LC}$ at maximum gross power.

a)



b)

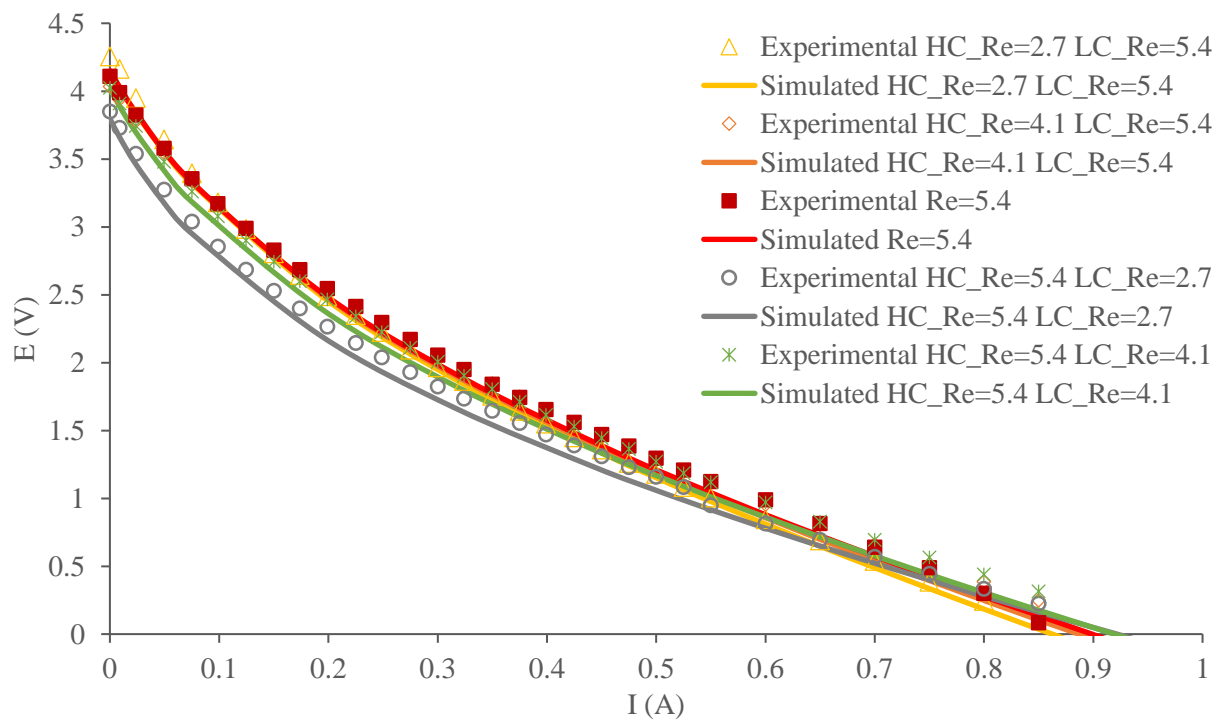


Fig. 6. Polarization curves a) $Q_{HC} = Q_{LC}$ b) $Q_{HC} \neq Q_{LC}$.

The gross power achieved at different flow rates is shown in Fig. 7 and Table 6. Maximum gross power values of 0.66 W and 0.70 W were obtained working with $Re=5.4$ and $Re=8.1$ respectively. Employing $Re=2.7$ and $Re=13.6$, practically the same value of maximum gross power is achieved (0.56 and 0.57 W respectively) due to a lower R_i in the first case, and higher voltage in the second situation. Furthermore, conditions with $Q_{HC} \neq Q_{LC}$ show higher influence of the low compartment flow rate as has been mentioned previously. The error accomplished at maximum gross power between experimental and simulated data is reported in Table 6. In all cases the gross power error is less than 8%, except for $Re=13.6$.

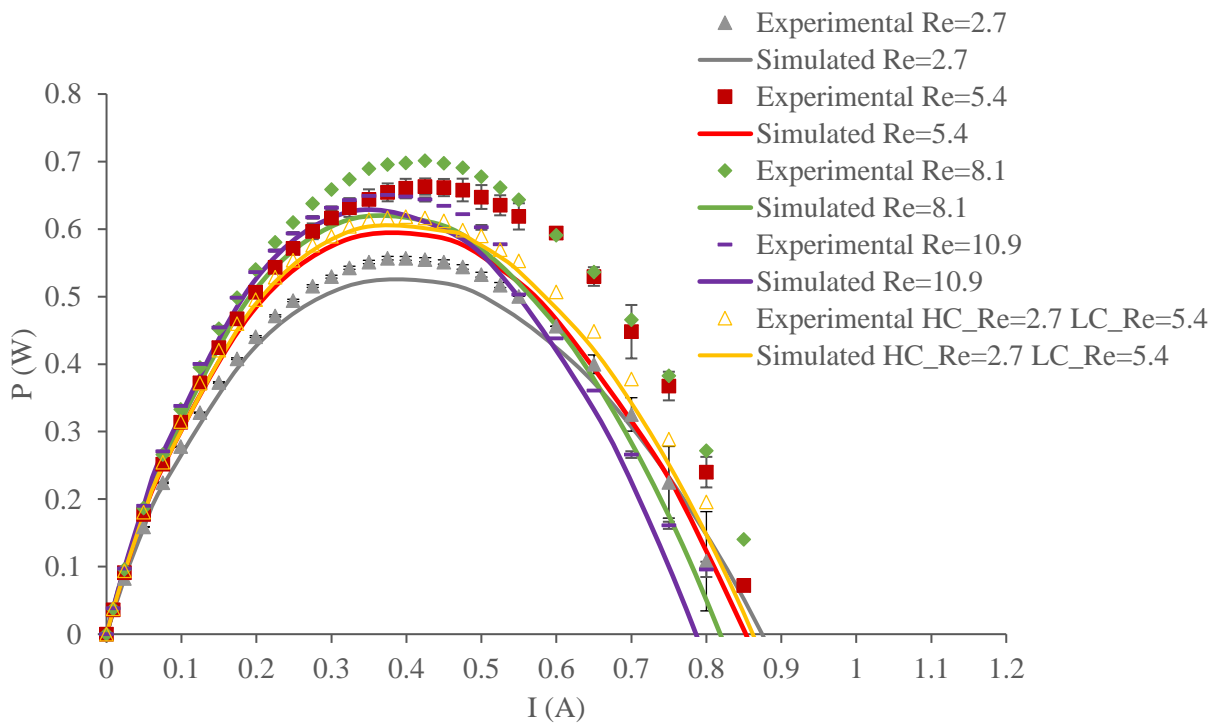


Fig. 7. Gross power vs current at different flow rates.

Table 6. Experimental and simulated maximum gross power under different Re numbers.

mL·min ⁻¹ (Re)	Exp. (W)	Sim. (W)	Error (%)
HC=LC=100 (2.7)	0.56	0.52	7.14
HC=LC=200 (5.4)	0.66	0.62	6.06
HC=LC=300 (8.1)	0.70	0.66	5.71
HC=LC=400 (10.9)	0.65	0.61	6.15
HC=LC=500 (13.6)	0.57	0.63	10.53
HC=100 LC=200 (2.7-5.4)	0.62	0.60	3.23
HC=150 LC=200 (4.1-5.4)	0.66	0.62	6.06
HC=200 LC=150 (5.4-4.1)	0.65	0.60	7.69
HC=200 LC=100 (5.4-2.7)	0.59	0.55	6.78

In order to determine the optimal flow rate, it is necessary to take into account pumping savings as well as the ease of working with low values of flow rate. Thus, in this work, as similar results of gross power were obtained working with Reynolds numbers of 5.4 and 8.1, the study of concentration and temperature influence was made working at Re=5.4.

3.2 Concentration

The influence of the concentration is analysed by flowing the following solutions through the HC and LC compartments keeping the concentration of NaCl in representative values of real streams: C1: seawater (0.66 M)/wastewater (0.0036 M); C2: brines (5 M)/brackish water (0.1 M); and C3: intermediate driving force (5 M-1 M). The use of high concentration solutions causes significant differences in the membrane behaviour. Membrane permselectivity values dramatically decrease when the concentration increases. In particular, Tedesco et al., (2015) reported a reduction down to 0.4-0.5 in α_{AEM} and α_{CEM} [12]. Previous works referred to specific membranes having better performance in the high salt concentration range at research stage [13]. Permselectivity was estimated using Aspen Custom Modeler when brines (5 M) were used in HC. Working with HC=5 M and LC=1 M the value estimated was for $\alpha=0.46$. On the other hand, when the low concentration was 0.1 M and the high compartment concentration remained constant, the permselectivity was $\alpha=0.68$.

The different experimental and simulated open circuit voltages achieved are shown in Table 7. The maximum OCV value was obtained when model seawater/wastewater solutions were used (4.11 V). In addition, when HC is kept constant, OCV increases as LC decreases. The error obtained was lower than 6% for the three different scenarios.

Table 7. Experimental and simulated OCV values at different scenarios.

Scenario	C (M)	Exp. (V)	Sim. (V)	Error (%)
Seawater/wastewater	C1: 0.66 M-0.0036 M	4.11	4.15	0.97
Brines/ brackish water	C2: 5 M-0.1 M	2.63	2.65	0.76
Intermediate	C3: 5 M-1 M	0.88	0.83	5.68

Fig. 8 shows the internal resistance values achieved using the three different concentration situations (5 M/1 M, 5 M/0.1 M and 0.66 M/ 0.0036 M). Seawater/wastewater scenario provokes higher values of internal resistance because the LC compartment has low conductivity. However, working with the other scenarios, R_i is negligible due to the increment in LC concentrations. Low compartment resistance is one and two order of magnitude lower when brines/brackish water and intermediate scenario respectively were used. At maximum gross power, R_{LC} values were $5.52 \cdot 10^{-3} \Omega \cdot m^2$.

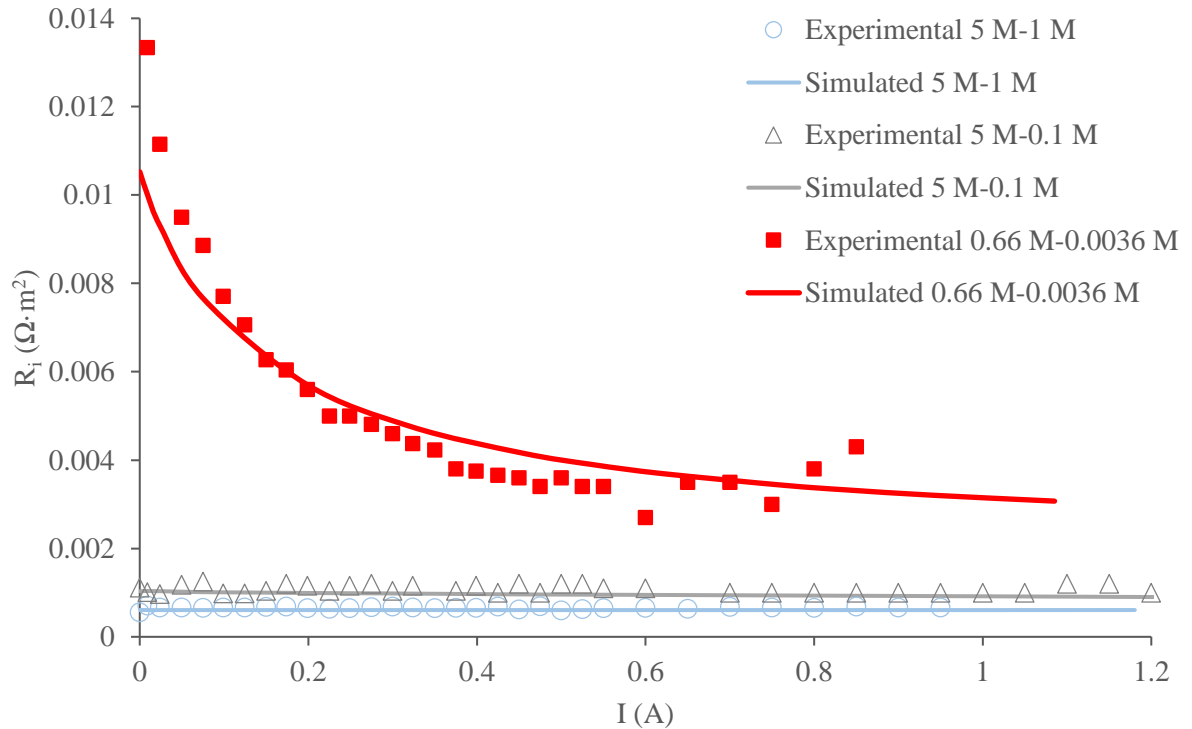


Fig. 8. R_i achieved at different concentration.

Fig. 9 shows the gross power (P) achieved at the different scenarios. In this way a greater range of possibilities for the model proposed in this work is offered. A maximum gross power of 1.6 W was reached working with the scenario C2 (5M – 0.1 M). On the other hand, using HC=5 M and LC=1 M, only around 0.3 W of gross power was achieved because for the same HC, the salinity gradient is lower in the second scenario, according to Nernst equation (Eq. 1). However, taking into account the relevance of the internal resistance, a trade-off between both factors is necessary to be considered. Regarding the limiting current, seawater/wastewater corresponding to scenario C1 reports the lowest value (0.9 A). On the other hand, working with higher LC concentrations, the internal resistance decreases and therefore the polarization curves depict lower slope; consequently, the limiting current grows up.

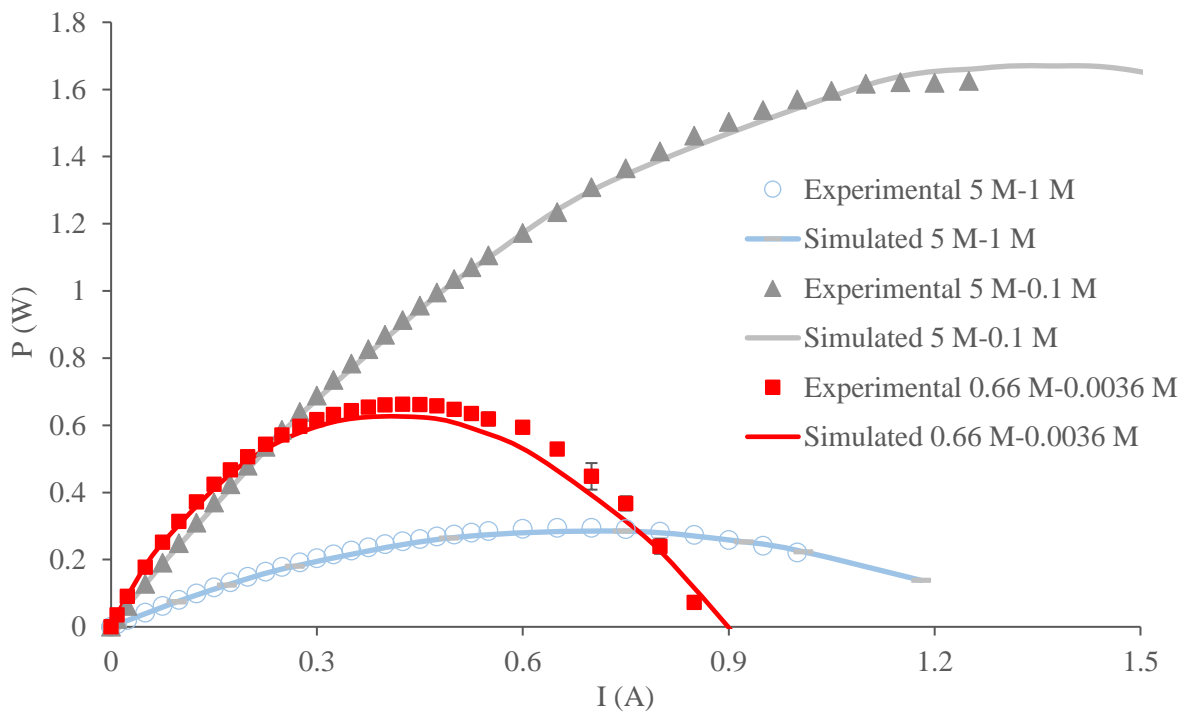


Fig. 9. Gross power vs current intensity at different scenarios.

3.3. Temperature

Water temperature in the sea or wastewaters from natural resources may experiment a seasonal change. Thus, the influence of this variable has been experimentally studied by performing experiments at 286 K, 291 K and 297±1 K with C1 solutions flowing at $Re=5.4$. To perform the simulations, the parameters reported in Table 3 were used. In addition, permselectivity values reported by the manufacturer were used. Previous works reported a dramatic decline in gross power when the temperature decreases [20,22,24]. The key to the diminution in gross power is the temperature influence in the ionic mobility and membrane resistance [24]. Ionic mobility decreases because the spacers block the transport [20]. Conductivity suffers a reduction around 2%/K when temperature decreases. This is due to the increase in R_{HC} and R_{LC} more significantly. On the other hand, membrane resistances were estimated. The estimated values of membrane resistance were $4 \cdot 10^{-4} \Omega \cdot m^2$ at 286 K and $2.5 \cdot 10^{-4} \Omega \cdot m^2$ at 291 K. Tufa et al., (2015) in the range 313 K to 293 K described an increase in membrane resistance of 178% and 87.5% for anionic and cationic exchange membrane respectively.

The difference between experimental and simulated OCV data is shown in Table 8. As can be seen, for high concentration and low concentration solutions of 0.66 M and 0.0036 M respectively and Reynolds number of 5.4, OCV decreases when temperature declines. OCV drops by 4.62 % from 297 K to 286 K beginning with 4.11 V lowering down to 3.92 V.

Table 8. Experimental and simulated OCV values at different temperatures.

T (K)	Exp. (V)	Sim. (V)	Error (%)
286±1 K	3.92	4.00	2.04
291±1 K	3.97	4.07	2.52
297±1 K	4.11	4.15	0.97

The contributions to the internal resistance (R_i) expressed as (%) at different temperatures are shown in Fig. 10. As can be seen, the ohmic resistance decreases as temperature increases. R_{mem} is the most affected contribution by temperature with values of 11.3%, 9.40% and 5.77% for 286 K, 291 K and 297 K respectively. In global terms, R_i suffers a reduction of 71% from $7.11 \cdot 10^{-3} \Omega \cdot m^2$ to $4.16 \cdot 10^{-3} \Omega \cdot m^2$ when temperature is increased

from 286 K to 297 K. This is mainly due to R_{LC} and R_{mem} values. At 286 K R_{LC} has a value of $5.41 \cdot 10^{-3} \Omega \cdot m^2$ while at 297 K the value is reduced to $2.52 \cdot 10^{-3} \Omega \cdot m^2$.

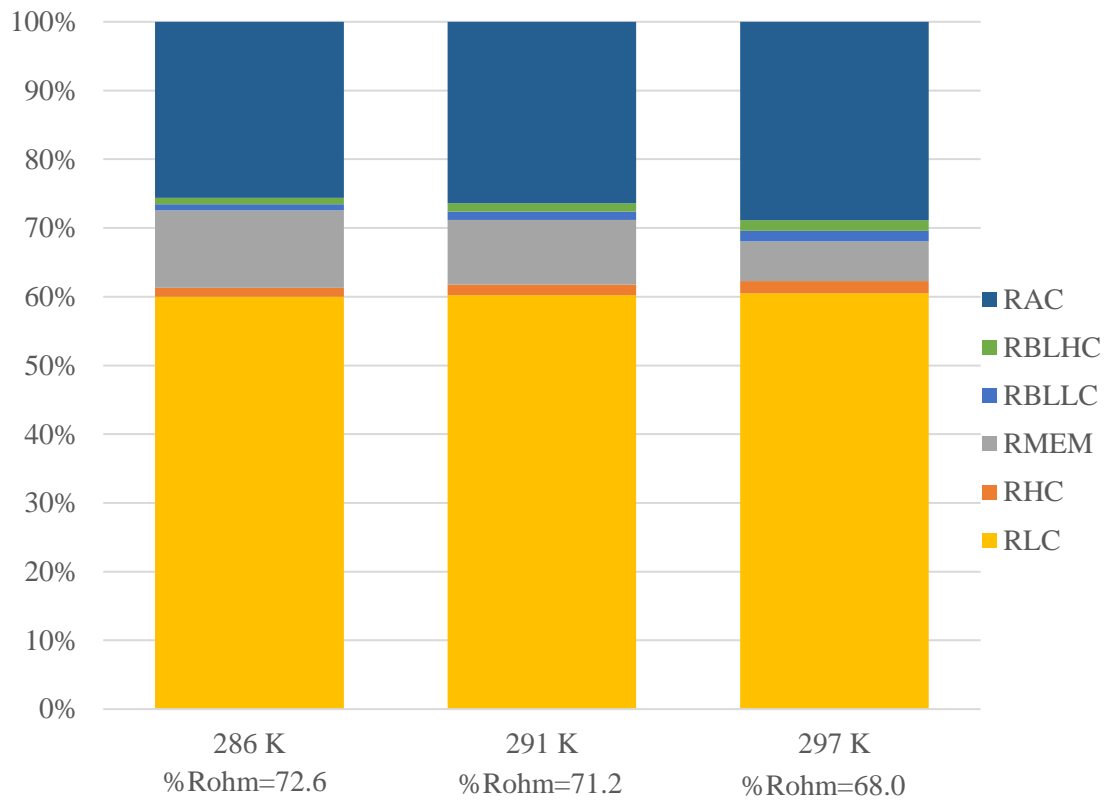


Fig. 10. Contributions to the internal resistance at different temperatures.

Fig. 11 shows the gross power against current intensity. At low current (up to 0.1 A), the curves are overlapped; however, as consequence of the product “E·I” (Eq. 5), when the current increases, the difference between gross power carried out at 286 K, 291 K and 297 K grows up. In addition, the limiting current decreases as the temperature declines. Values of 0.39 W, 0.47W and 0.66 W of gross power were obtained for 286 K, 291 K and 297±1 K respectively, decreasing by 41% from the maximum to the minimum temperature. Kingsbury et al., (2009) and Tufa et al., (2015) reported an increment of 30% when the temperature increases from 283 to 293 K. Thus, the values obtained in this work are in concordance with previous literature.

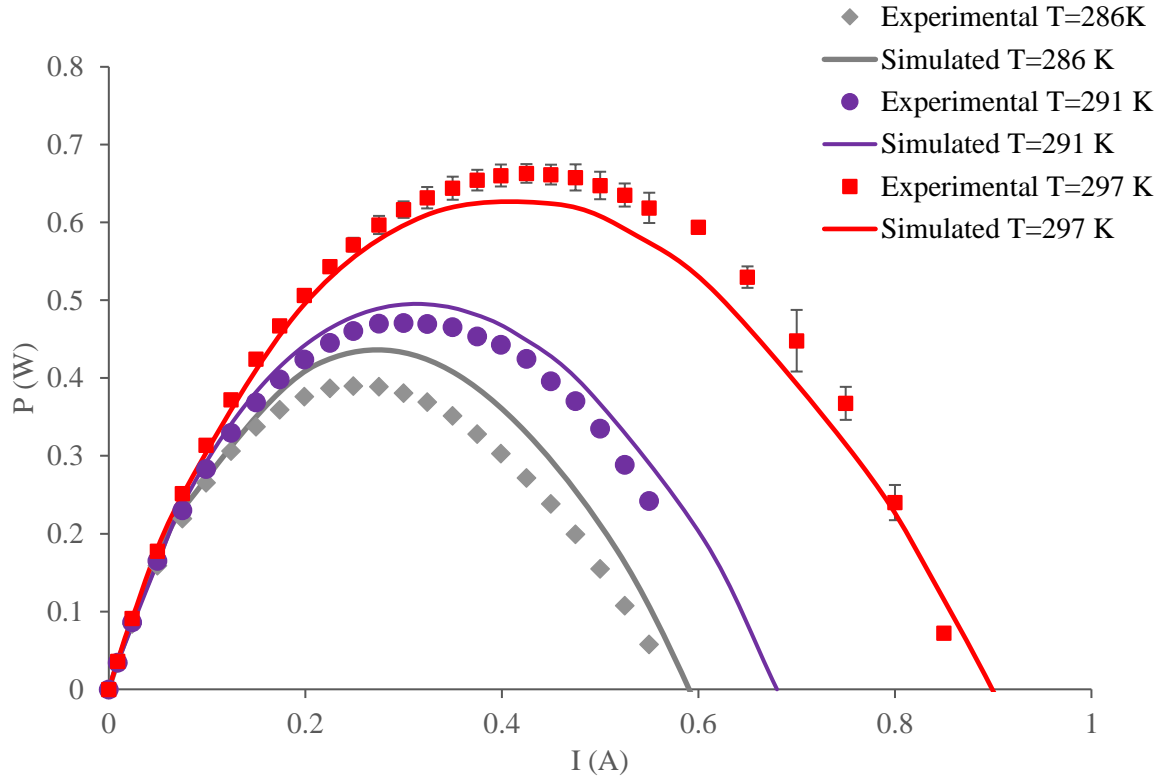


Fig. 11. Effect of temperature on gross power. Experimental (points) and simulated (lines).

3.4 Model Validation

In order to validate the model proposed in the present work a parity graph has been performed (Fig. 12). The parity graph includes the comparison between experimental and simulated voltage data from this work and literature [34,35] at different flow rates, concentration and temperature. As depicted in Fig. 12, the results are within an error range of 15%. The highest proportion of values fall on the bisection line implying a good match between the model and the laboratory results.

The global error from the results of this work is 7.88%. This value was calculated with the weighted standard deviation according to Eq. 17.

$$\sigma = \sqrt{\frac{\sum_{i=1}^n \left(\frac{E_{Exp}(V) - E_{Sim}(V)}{E_{Exp}(V)} \right)^2}{n - 1}} \quad (17)$$

Where E_{Exp} (V) and E_{Sim} (V) are the experimental and simulated voltage values respectively and n is the total number of experiments carried out. These results assess the

reliability of the mathematical model to describe the experimental behaviour of the laboratory scale plant using synthetic waters.

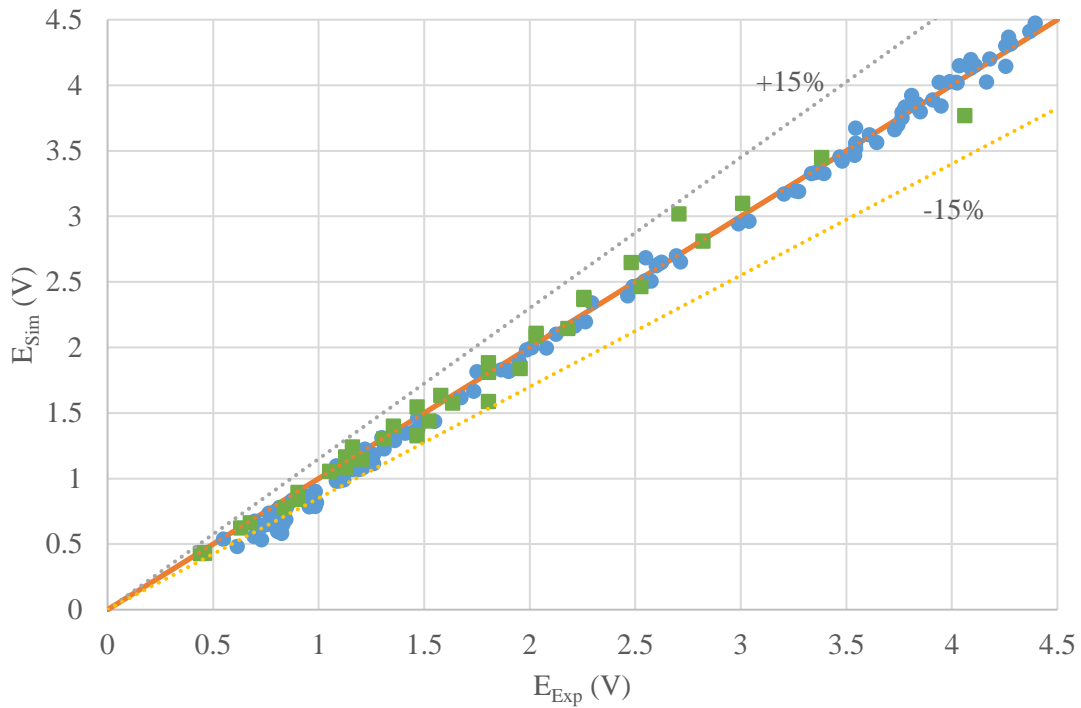


Fig. 12. Parity plot comparing simulated and experimental voltage. This work (●) and literature data (■) [34,35].

Thus, we conclude that the model proposed is an accurate tool to preliminary predict the influence of operational variables on the energy recovery potential of this technology as well as an outstanding resource for future scaling up of RED plants.

Conclusions

Recovery of the energy contained in SGP is largely dependent on the technology characteristics and the operation conditions. Having selected RED as the main technology, variables such as concentration driving force created by the characteristics of the concentrate and dilute solutions, temperature of the solutions due to seasonal variations and flow rate inside the stacks that determines the fluid dynamics and the residence time, strongly determine the results in terms of gross power. Thus, we report a tool based on the development of a phenomenological model that gives preliminary information on the maximum energy recovery and helps making the selection of the operating conditions at different scenarios. The model has been assessed against

experimental results working with a commercial membrane in a lab-scale RED stack and highlights the main influence of feed flow rate, concentration and temperature in the performance of SGE-RED systems.

Acknowledgements

Financial support from Community of Cantabria - Regional Plan for the project: Gradisal “RM16-XX-046-SODERCAN/FEDER” is gratefully acknowledged. Moreover, authors acknowledge Spanish Ministry of Economy and Competitiveness for the projects CTM2015-66078-R, CTM2014-57833-R and CTM2017-87850-R and Dr. Jordi Carrillo for his advice and technical support.

Nomenclature

A	Area of one membrane (m^2)
b	Cell Width (m)
C	Salt concentration ($\text{mol}\cdot\text{m}^3$)
cond_{HC}	Conductivity in high compartment ($\text{S}\cdot\text{m}^{-1}$)
cond_{LC}	Conductivity in low compartment ($\text{S}\cdot\text{m}^{-1}$)
D_{h}	Hydraulic diameter (m)
$D_{\text{H}_2\text{O}}$	Water diffusivity ($\text{m}^2\cdot\text{s}^{-1}$)
D_{NaCl}	Salt diffusivity ($\text{m}^2\cdot\text{s}^{-1}$)
E_{cell}	Cell pair voltage (V)
E_{Exp}	Experimental voltage (V)
E_{Sim}	Simulated voltage (V)
F	Faraday's constant ($96,485 \text{ C mol}^{-1}$)
I	Current (A)
J	Current density ($\text{A}\cdot\text{m}^{-2}$)
$J_{\text{H}_2\text{O}}$	Osmotic flux ($\text{mol}\cdot\text{m}^{-2}\cdot\text{s}^{-1}$)
J_{Cl^-}	Cl^- flux ($\text{mol}\cdot\text{m}^{-2}\cdot\text{s}^{-1}$)
J_{Na^+}	Na^+ flux ($\text{mol}\cdot\text{m}^{-2}\cdot\text{s}^{-1}$)
L	Cell Length (m)
N_{cell}	Number of cell pairs (-)
P	Gross power (W)
Q	Volumetric flow rate per cell ($\text{m}^3\cdot\text{s}^{-1}$)
R	Universal gas constant ($8.314 \text{ J}\cdot\text{mol}^{-1}\cdot\text{K}^{-1}$)
R_{AC}	Concentration change in the bulk solution Resistance ($\Omega\cdot\text{m}^2$)
R_{AEM}	Anionic Membrane Resistance ($\Omega\cdot\text{m}^2$)
R_{BL}	Boundary Layer Resistance ($\Omega\cdot\text{m}^2$)

R_{CEM}	Cationic Membrane Resistance ($\Omega \cdot m^2$)
Re	Reynolds number (-)
R_{HC}	High Concentration Solution Resistance ($\Omega \cdot m^2$)
R_i	Internal Resistance ($\Omega \cdot m^2$)
R_L	External Load Resistance ($\Omega \cdot m^2$)
R_{LC}	Low Concentration Solution Resistance ($\Omega \cdot m^2$)
R_{mem}	Average Membrane Resistance ($\Omega \cdot m^2$)
$R_{non-ohmic}$	Non-ohmic Resistance ($\Omega \cdot m^2$)
R_{ohmic}	Ohmic Resistance ($\Omega \cdot m^2$)
R_{stack}	Total Internal Resistance ($\Omega \cdot m^2$)
T	Temperature (K)
tr	Residence Time (s)
E	Total Voltage (V)
v	Linear velocity ($m \cdot s^{-1}$)
V_{H_2O}	Molar volume ($1.8 \cdot 10^{-5} m^3 \cdot mol^{-1}$)
z	Valence

Greek Letters

α	Average permselectivity (-)
α_{AEM}	Anion membrane permselectivity (-)
α_{CEM}	Cation membrane permselectivity (-)
γ	Activity coefficient (-)
δ	Intermembrane distance (m)
δ_m	Membrane Thickness (m)
ϵ	Porosity (-)
ρ	Density of waters ($kg \cdot m^{-3}$)

μ	Dynamic viscosity ($\text{kg}\cdot\text{m}^{-1}\cdot\text{s}^{-1}$)
-------	---

Abbreviation

AEM	Anion Exchange Membrane
CEM	Cation Exchange Membrane
ED	Conventional Electrodialysis
ERS	Electrode Rinse Solution
IEM	Ion Exchange Membrane
OCV	Open Circuit Voltage
PES	Polyethersulfone
RED	Reverse Electrodialysis
SG	Salinity Gradient
SGP	Salinity Gradient Power
WWTP	Wastewater Treatment Plant

Subscript

HC	High Concentrated Solution
LC	Low Concentrated Solution

References

- [1] R.A. Tufa, E. Curcio, W. van Baak, J. Veerman, S. Grasman, E. Fontananova, G. Di Profio, Potential of brackish water and brine for energy generation by salinity gradient power-reverse electrodialysis (SGP-RE), *RSC Adv.* 4 (2014) 42617–42623. doi:10.1039/C4RA05968A.
- [2] A.H. Avci, P. Sarkar, R.A. Tufa, D. Messana, P. Argurio, E. Fontananova, G. Di Profio, E. Curcio, Effect of Mg 2+ ions on energy generation by Reverse Electrodialysis, *J. Memb. Sci.* 520 (2016) 499–506. doi:10.1016/j.memsci.2016.08.007.
- [3] J. Veerman, M. Saakes, S.J. Metz, G.J. Harmsen, Reverse electrodialysis: Performance of a stack with 50 cells on the mixing of sea and river water, *J. Memb. Sci.* 327 (2009) 136–144. doi:10.1016/j.memsci.2008.11.015.
- [4] J.W. Post, H.V.M. Hamelers, C.J.N. Buisman, Energy recovery from controlled mixing salt and fresh water with a reverse electrodialysis system, *Environ. Sci. Technol.* 42 (2008) 5785–5790. doi:10.1021/es8004317.
- [5] J.W. Post, Blue Energy: electricity production from salinity gradients by reverse electrodialysis, (PhD Thesis), Wageningen University, 2009.
- [6] E. Fontananova, D. Messana, R.A. Tufa, I. Nicotera, V. Kosma, E. Curcio, W. van Baak, E. Drioli, G. Di Profio, Effect of solution concentration and composition on the electrochemical properties of ion exchange membranes for energy conversion, *J. Power Sources.* 340 (2017) 282–293. doi:10.1016/j.jpowsour.2016.11.075.
- [7] M. Tedesco, C. Scalici, D. Vaccari, A. Cipollina, A. Tamburini, G. Micale, Performance of the first reverse electrodialysis pilot plant for power production from saline waters and concentrated brines, *J. Memb. Sci.* 500 (2016) 33–45. doi:10.1016/j.memsci.2015.10.057.
- [8] A. Tamburini, G. La Barbera, A. Cipollina, G. Micale, M. Ciofalo, CFD prediction of scalar transport in thin channels for reverse electrodialysis, *Desalin. Water Treat.* 55 (2015) 3424–3445. doi:10.1080/19443994.2014.959735.

- [9] Y. Mei, C.Y. Tang, Recent developments and future perspectives of reverse electro dialysis technology: A review, *Desalination*. 425 (2018) 156–174. doi:10.1016/j.desal.2017.10.021.
- [10] C. Fernandez-Gonzalez, A. Dominguez-Ramos, R. Ibañez, Y. Chen, A. Irabien, Valorization of desalination brines by electro dialysis with bipolar membranes using nanocomposite anion exchange membranes, *Desalination*. 406 (2017) 16–24. doi:10.1016/j.desal.2016.07.033.
- [11] D.A. Vermaas, M. Saakes, K. Nijmeijer, Doubled power density from salinity gradients at reduced intermembrane distance, *Environ. Sci. Technol.* 45 (2011) 7089–7095. doi:10.1021/es2012758.
- [12] M. Tedesco, E. Brauns, A. Cipollina, G. Micale, P. Modica, G. Russo, J. Helsen, Reverse electro dialysis with saline waters and concentrated brines: A laboratory investigation towards technology scale-up, *J. Memb. Sci.* 492 (2015) 9–20. doi:10.1016/j.memsci.2015.05.020.
- [13] M. Tedesco, A. Cipollina, A. Tamburini, G. Micale, Towards 1 kW power production in a reverse electro dialysis pilot plant with saline waters and concentrated brines, *J. Memb. Sci.* 522 (2017) 226–236. doi:10.1016/j.memsci.2016.09.015.
- [14] J. Veerman, M. Saakes, S.J. Metz, G.J. Harmsen, Electrical power from sea and river water by reverse electro dialysis: A first step from the laboratory to a real power plant, *Environ. Sci. Technol.* 44 (2010) 9207–9212. doi:10.1021/es1009345.
- [15] D.A. Vermaas, J. Veerman, M. Saakes, K. Nijmeijer, Influence of multivalent ions on renewable energy generation in reverse electro dialysis, *Energy Environ. Sci.* 7 (2014) 1434–1445. doi:10.1039/C3EE43501F.
- [16] J. Veerman, D.A. Vermaas, Reverse electro dialysis: Fundamentals, in: *Sustain. Energy from Salin. Gradients*, Elsevier Ltd., 2016: pp. 77–133. doi:10.1016/B978-0-08-100312-1.00004-3.
- [17] J. Veerman, M. Saakes, S.J. Metz, G.J. Harmsen, Reverse electro dialysis: Evaluation of suitable electrode systems, *J. Appl. Electrochem.* 40 (2010) 1461–

1474. doi:10.1007/s10800-010-0124-8.
- [18] J.W. Post, J. Veerman, H.V.M. Hamelers, G.J.W. Euverink, S.J. Metz, K. Nymeijer, C.J.N. Buisman, Salinity-gradient power: Evaluation of pressure-retarded osmosis and reverse electrodialysis, *J. Memb. Sci.* 288 (2007) 218–230. doi:10.1016/j.memsci.2006.11.018.
- [19] A. Cipollina, G. Micale, A. Tamburini, M. Tedesco, L. Gurreri, J. Veerman, S. Grasman, Reverse electrodialysis: Applications, in: *Sustain. Energy from Salinity Gradients*, Elsevier Ltd., 2016: pp. 135–180. doi:10.1016/B978-0-08-100312-1.00005-5.
- [20] R.S. Kingsbury, F. Liu, S. Zhu, C. Boggs, M.D. Armstrong, D.F. Call, O. Coronell, Impact of natural organic matter and inorganic solutes on energy recovery from five real salinity gradients using reverse electrodialysis, *J. Memb. Sci.* 541 (2017) 621–632. doi:10.1016/j.memsci.2017.07.038.
- [21] A. Daniilidis, R. Herber, D.A. Vermaas, Upscale potential and financial feasibility of a reverse electrodialysis power plant, *Appl. Energy*. 119 (2014) 257–265. doi:10.1016/j.apenergy.2013.12.066.
- [22] A. Daniilidis, D.A. Vermaas, R. Herber, K. Nijmeijer, Experimentally obtainable energy from mixing river water, seawater or brines with reverse electrodialysis, *Renew. Energy*. 64 (2014) 123–131. doi:10.1016/j.renene.2013.11.001.
- [23] R.A. Tufa, E. Rugiero, D. Chanda, J. Hnàt, W. van Baak, J. Veerman, E. Fontananova, G. Di Profio, E. Drioli, K. Bouzek, E. Curcio, Salinity gradient power-reverse electrodialysis and alkaline polymer electrolyte water electrolysis for hydrogen production, *J. Memb. Sci.* 514 (2016) 155–164. doi:10.1016/j.memsci.2016.04.067.
- [24] R.A. Tufa, E. Curcio, E. Brauns, W. van Baak, E. Fontananova, G. Di Profio, Membrane Distillation and Reverse Electrodialysis for Near-Zero Liquid Discharge and low energy seawater desalination, *J. Memb. Sci.* 496 (2015) 325–333. doi:10.1016/j.memsci.2015.09.008.
- [25] S. Pawlowski, J.G. Crespo, S. Velizarov, Pressure drop in reverse electrodialysis: Experimental and modeling studies for stacks with variable number of cell pairs,

- J. Memb. Sci. 462 (2014) 96–111. doi:10.1016/j.memsci.2014.03.020.
- [26] B. Zhang, H. Gao, Y. Chen, Enhanced Ionic Conductivity and Power Generation Using Ion-Exchange Resin Beads in a Reverse-Electrodialysis Stack, *Environ. Sci. Technol.* 49 (2015) 14717–14724. doi:10.1021/acs.est.5b03864.
- [27] H. Susanto, M. Fitrianingtyas, A.M. Samsudin, A. Syakur, Experimental study of the natural organic matters effect on the power generation of reverse electrodialysis, *Int. J. Energy Res.* 41 (2017). doi:10.1002/er.3728.
- [28] Y.M. Chao, T.M. Liang, A feasibility study of industrial wastewater recovery using electrodialysis reversal, *Desalination.* 221 (2008) 433–439. doi:10.1016/j.desal.2007.04.065.
- [29] P.E. Dlugolecki, Spacer, cell and device for an ion-exchanging process and method therefore, WO Patent No. 104381 A2, 2010.
- [30] W. van Baak, J. Van Engelen, D.M. Sterescu, Process for preparing membranes, WO Patent No. 007399 A1, 2010.
- [31] Juchui Ray Lin, Jenny Lin, Process for making a monomer solution for making cation exchange membranes, US Patent No. 0317128 A1, 2013.
- [32] V.S. Sawant, J.H. Barber, R. Harikrishnan, V. Sridharan, Electrodialysis spacer and stack, US Patent No. 0310902 A1, 2016.
- [33] R. Van Engelen, Process for preparing composite membranes, WO Patent No. 106357 A1, 2010.
- [34] P. Długolecki, A. Gambier, K. Nijmeijer, M. Wessling, Practical Potential of Reverse Electrodialysis As Process for Sustainable Energy Generation, *Environ. Sci. Technol.* 43 (2009) 6888–6894. doi:10.1021/es9009635.
- [35] M. Tedesco, A. Cipollina, A. Tamburini, I.D.L. Bogle, G. Micale, A simulation tool for analysis and design of reverse electrodialysis using concentrated brines, *Chem. Eng. Res. Des.* 93 (2015) 441–456. doi:10.1016/j.cherd.2014.05.009.
- [36] D.A. Vermaas, M. Saakes, K. Nijmeijer, Early detection of preferential channeling in reverse electrodialysis, *Electrochim. Acta.* 117 (2014) 9–17.

doi:10.1016/j.electacta.2013.11.094.

- [37] P. Długołęcki, J. Dabrowska, K. Nijmeijer, M. Wessling, Ion conductive spacers for increased power generation in reverse electrodialysis, *J. Memb. Sci.* 347 (2010) 101–107. doi:10.1016/j.memsci.2009.10.011.
- [38] A. D'Angelo, M. Tedesco, A. Cipollina, A. Galia, G. Micale, O. Scialdone, Reverse electrodialysis performed at pilot plant scale: Evaluation of redox processes and simultaneous generation of electric energy and treatment of wastewater, *Water Res.* 125 (2017) 123–131. doi:10.1016/j.watres.2017.08.008.
- [39] J.G. Hong, W. Zhang, J. Luo, Y. Chen, Modeling of power generation from the mixing of simulated saline and freshwater with a reverse electrodialysis system: The effect of monovalent and multivalent ions, *Appl. Energy.* 110 (2013) 244–251. doi:10.1016/j.apenergy.2013.04.015.
- [40] J. Gi Hong, Y. Chen, Evaluation of electrochemical properties and reverse electrodialysis performance for porous cation exchange membranes with sulfate-functionalized iron oxide, *J. Memb. Sci.* 473 (2015) 210–217. doi:10.1016/j.memsci.2014.09.012.
- [41] M. Tedesco, A. Cipollina, A. Tamburini, W. van Baak, G. Micale, Modelling the Reverse ElectroDialysis process with seawater and concentrated brines, *Desalin. Water Treat.* 49 (2012) 404–424. doi:10.1080/19443994.2012.699355.
- [42] S. Pawlowski, T. Rijnaarts, M. Saakes, K. Nijmeijer, J.G. Crespo, S. Velizarov, Improved fluid mixing and power density in reverse electrodialysis stacks with chevron-profiled membranes, *J. Memb. Sci.* 531 (2017) 111–121. doi:10.1016/j.memsci.2017.03.003.
- [43] D.A. Vermaas, M. Saakes, K. Nijmeijer, Enhanced mixing in the diffusive boundary layer for energy generation in reverse electrodialysis, *J. Memb. Sci.* 453 (2014) 312–319. doi:10.1016/j.memsci.2013.11.005.
- [44] X. Zhu, W. He, B.E. Logan, Reducing pumping energy by using different flow rates of high and low concentration solutions in reverse electrodialysis cells, *J. Memb. Sci.* 486 (2015) 215–221. doi:10.1016/j.memsci.2015.03.035.

- [45] E. Brauns, Salinity gradient power by reverse electrodialysis: effect of model parameters on electrical power output, *Desalination*. 237 (2009) 378–391. doi:10.1016/j.desal.2008.10.003.
- [46] E. Fontananova, W. Zhang, I. Nicotera, C. Simari, W. van Baak, G. Di Profio, E. Curcio, E. Drioli, Probing membrane and interface properties in concentrated electrolyte solutions, *J. Memb. Sci.* 459 (2014) 177–189. doi:10.1016/j.memsci.2014.01.057.
- [47] J. Veerman, M. Saakes, S.J. Metz, G.J. Harmsen, Reverse electrodialysis: A validated process model for design and optimization, *Chem. Eng. J.* 166 (2011) 256–268. doi:10.1016/j.cej.2010.10.071.
- [48] M. Tedesco, H.V.M. Hamelers, P.M. Biesheuvel, Nernst-Planck transport theory for (reverse) electrodialysis: I. Effect of co-ion transport through the membranes, *J. Memb. Sci.* 510 (2016) 370–381. doi:10.1016/j.memsci.2016.03.012.
- [49] E. Farrell, M.I. Hassan, R.A. Tufa, A. Tuomiranta, A.H. Avci, A. Politano, E. Curcio, H.A. Arafat, Reverse electrodialysis powered greenhouse concept for water- and energy-self-sufficient agriculture, *Appl. Energy*. 187 (2017) 390–409. doi:10.1016/j.apenergy.2016.11.069.
- [50] L. Gurreri, A. Tamburini, A. Cipollina, G. Micale, CFD analysis of the fluid flow behavior in a reverse electrodialysis stack, *Desalin. Water Treat.* 48 (2012) 390–403. doi:10.1080/19443994.2012.705966.
- [51] Z. Cao, D.E. Wiley, A.G. Fane, CFD simulations of net-type turbulence promoters in a narrow channel, *J. Memb. Sci.* 185 (2001) 157–176. doi:10.1016/S0376-7388(00)00643-8.
- [52] B. Zhang, J.G. Hong, S. Xie, S. Xia, Y. Chen, An integrative modeling and experimental study on the ionic resistance of ion-exchange membranes, *J. Memb. Sci.* 524 (2017) 362–369. doi:10.1016/j.memsci.2016.11.050.
- [53] A.A. Moya, Numerical simulation of ionic transport processes through bilayer ion-exchange membranes in reverse electrodialysis stacks, *J. Memb. Sci.* 524 (2017) 400–408. doi:10.1016/j.memsci.2016.11.051.

- [54] D.A. Vermaas, E. Guler, M. Saakes, K. Nijmeijer, Theoretical power density from salinity gradients using reverse electrodialysis, *Energy Procedia*. 20 (2012) 170–184. doi:10.1016/j.egypro.2012.03.018.
- [55] J.G. Hong, B. Zhang, S. Glabman, N. Uzal, X. Dou, H. Zhang, X. Wei, Y. Chen, Potential ion exchange membranes and system performance in reverse electrodialysis for power generation: A review, *J. Memb. Sci.* 486 (2015) 71–88. doi:10.1016/j.memsci.2015.02.039.
- [56] K.S. Pitzer, Thermodynamics of electrolytes. I. Theoretical basis and general equations, *J. Phys. Chem.* 77 (1973) 268–277. doi:10.1021/j100621a026.
- [57] D.A. Vermaas, M. Saakes, K. Nijmeijer, Power generation using profiled membranes in reverse electrodialysis, *J. Memb. Sci.* 385–386 (2011) 234–242. doi:10.1016/j.memsci.2011.09.043.
- [58] J. Veerman, R.M. de Jong, M. Saakes, S.J. Metz, G.J. Harmsen, Reverse electrodialysis: Comparison of six commercial membrane pairs on the thermodynamic efficiency and power density, *J. Memb. Sci.* 343 (2009) 7–15. doi:10.1016/j.memsci.2009.05.047.